Supersonic Far-Field Boundary Conditions for Transonic Small-Disturbance Theory

Michael D. Gibbons*
Planning Research Corporation, PRC Systems Services, Hampton, Virginia 23666
and
John T. Batina†
NASA Langley Research Center, Hampton, Virginia 23665

Characteristic far-field boundary conditions for supersonic freestream flow have been developed and implemented within a transonic small-disturbance code. The boundary conditions have been implemented within the CAP-TSD code (Computational Aeroelasticity Program – Transonic Small Disturbance), which has been developed recently for aeroelastic analysis of complete aircraft configurations. These boundary conditions improve the accuracy of the solutions for supersonic freestream applications. They also allow the extent of the grid to be much smaller, thus providing savings in the computational time required to obtain solutions. Comparisons are shown between surface pressures computed using large and small grid extents for the NACA 0012 airfoil and the F-5 wing at various Mach numbers and angles of attack. Both steady and unsteady results are presented and comparisons are made with Euler results and with experimental data to assess the accuracy of the new far-field boundary conditions. Comparisons of these results show that the supersonic boundary conditions allow a much smaller grid to be used without losing accuracy.

Nomenclature

a	= local speed of sound
c_r	= root chord
k	= reduced frequency, $\omega c_r/2U$
M	= local Mach number
M_∞	= freestream Mach number
n_x, n_y, n_z	= normal components to Mach cone
s	= distance measured along a Mach line
t	= time
U	= freestream speed
u, v, w	= Cartesian velocity components
x, y, z	= Cartesian coordinate in freestream, spanwise, and vertical directions, respectively
x_p	= pitch axis
α_m	= mean angle of attack
α_o	= oscillation amplitude
β	= similarity parameter, $\sqrt{M^2-1}$
γ	= ratio of specific heats
Φ	= full potential
ϕ	= small-disturbance potential
ω	= angular frequency

Received Feb. 25, 1989; presented as Paper 89-1283 at the AIAA/ASME/ASCE/AHS/ASC 30th Structures, Structural Dynamics, and Materials Conference, Mobile, AL, April 3-5, 1989; revision received Oct. 31, 1989.

*Research Scientist, Advanced Aircraft Projects, Aeroelasticity Division. Member AIAA.

†Senior Research Scientist, Unsteady Aerodynamics Branch, Structural Dynamics Division. Senior Member AIAA.

Introduction

OVER the past several years there has been considerable progress in the development of methods for the prediction of unsteady transonic flows. A survey of these computational methods with emphasis on use for aeroelastic problems was reported by Edwards and Thomas.[1] The ability to accurately calculate unsteady flows is particularly important in the field of aeroelasticity. Aeroelastic instabilities such as flutter and divergence, for example, are very sensitive to nonlinear effects such as thickness and moving shock waves. An accurate calculation of these unsteady transonic flows is critical to determining flutter conditions.

An example of one of the most fully developed computer codes for unsteady aeroelastic analysis in the transonic Mach number regime is the CAP-TSD[2] code (Computational Aeroelasticity Program—Transonic Small Disturbance). CAP-TSD solves the unsteady transonic small-disturbance equation by a time-accurate approximate factorization algorithm. The code can treat complete aircraft configurations consisting of an arbitrary combination of bodies and lifting surfaces. Examples of some complete aircraft calculations including results for the General Dynamics F-16 aircraft are given by Batina et al.[2] Also recently included in the CAP-TSD code are the effects of shock-generated entropy and vorticity,[3] thus giving Euler-like solutions while retaining the relative simplicity and cost efficiency of the small-disturbance potential formulation.

CAP-TSD has been used primarily to calculate transonic flows with a subsonic freestream, although supersonic freestream results have been reported by Bennett et al.[4] However, these calculations were performed using a relatively large grid extent in order to minimize the effects of the outer boundary conditions on the near-field flow and, hence, on the surface pressures. In Ref. 4, a no-flow-through boundary condition was used along the outer boundaries.

The purpose of this paper is to report on the implementation of a characteristic far-field boundary condition in CAP-TSD for supersonic freestream applications. The objective of the study was to improve the accuracy and efficiency of the code for such applications. The efficiency may be improved by

minimizing the grid extent and thus reducing the computational cost. This paper gives a description of the new supersonic far-field boundary conditions along with results and comparisons that assess the capability.

Governing Equation

The governing flow equation solved by CAP-TSD is the unsteady transonic small-disturbance equation. The basic assumptions in deriving this equation are isentropic, irrotational, and inviscid flow and only small perturbations in the freestream flow are allowed. The TSD equation may be expressed in conservation law form as

$$\frac{\partial}{\partial t}\left(-A\phi_t - B\phi_x\right) + \frac{\partial}{\partial x}\left(E\phi_x + F\phi_x^2 + G\phi_y^2\right) + \frac{\partial}{\partial y}\left(\phi_y + H\phi_x\phi_y\right) + \frac{\partial}{\partial z}\left(\phi_z\right) = 0 \tag{1}$$

where the constants A, B, and E are defined by

$$A = M_\infty^2, \qquad B = 2M_\infty^2, \qquad E = 1 - M_\infty^2 \tag{2}$$

The choices for F, G, and H used in the present study are

$$F = -\tfrac{1}{2}(\gamma+1)M_\infty^2, \qquad G = \tfrac{1}{2}(\gamma-3)M_\infty^2, \qquad H = -(\gamma-1)M_\infty^2 \tag{3}$$

The TSD equation is solved by a time-accurate approximate factorization (AF) algorithm, which has excellent numerical stability characteristics. An important feature of the AF algorithm is the ease with which new boundary conditions or the addition of higher-order terms may be incorporated.

Original Boundary Conditions

The boundary conditions used previously for applications involving supersonic freestream[4] are given by

Upstream:

$$\phi = 0 \tag{4a}$$

Downstream:

$$\phi_x = 0 \tag{4b}$$

Above/below:

$$\phi_z = 0 \tag{4c}$$

Far spanwise:

$$\phi_y = 0 \tag{4d}$$

Symmetry plane:

$$\phi_y = 0 \tag{4e}$$

The boundary conditions [Eqs. (4c) and (4d)] represent a no-flow-through boundary condition. Physically, such far-field boundary conditions represent walls surrounding the model and may allow waves that are incident on the boundaries to reflect back into the near field for certain Mach numbers and grid extents. Previously, the no-flow-through boundary conditions were the only ones available for supersonic freestreams. Plane-wave-type nonreflecting boundary conditions for subsonic freestreams similar to that of Kwak[5] are also available as an option within the CAP-TSD code.[6]

Supersonic Boundary Conditions

The supersonic boundary conditions developed in the present study were derived using the method of characteristics.[7] The method transforms a set of differential equations into a system of partial differential equations that are valid only on a surface called a characteristic surface in three dimensions or characteristic curves in two dimensions. Thus, for each characteristic surface there is a partial differential equation valid only on that surface. This partial differential equation is also called the compatibility equation. The compatibility equation specifies the flow conditions anywhere on the characteristic surface and, hence, can be used to determine the required boundary conditions. This method was developed herein by applying it to the three-dimensional steady full-potential equation rather than the TSD equation because the full-potential function Φ includes the complete flowfield effects, whereas the TSD potential function ϕ represents only part of the solution; that is, the freestream effects must be added back into the solution. The equations for which the method of characteristics was applied are the three-dimensional steady full-potential equation and the conditions of zero vorticity given by

$$u_x(a^2-u^2) + v_y(a^2-v^2) + w_z(a^2-w^2) - uv(u_y+v_x) - vw(v_z+w_y) - wu(w_x+u_z) = 0 \tag{5a}$$

$$u_z - w_x = 0 \tag{5b}$$

$$v_x - u_y = 0 \tag{5c}$$

where the Cartesian velocity components are defined by

$$u = \frac{\partial\Phi}{\partial x}, \qquad v = \frac{\partial\Phi}{\partial y}, \qquad w = \frac{\partial\Phi}{\partial z}$$

In Eq. (5a), the variable a is the local speed of sound. The compatibility equation for Eqs. (5a–5c) can be written as

$$u_x(1-M^2) + (n_y/n_x)u_y + (n_z/n_x)u_z - (n_y/n_x)v_x + v_y - (n_z/n_x)w_x + w_z = 0 \tag{6}$$

where the streamlines are assumed to be parallel to the x axis, which is consistent with the small-disturbance approximation. The quantities n_x, n_y, and n_z represent the components of the unit normal to the characteristic surface (see Fig. 1) and are determined by the following two equations

$$n_x^2 + n_y^2 + n_z^2 = 1 \tag{7a}$$

$$(1-M^2)n_x^2 + n_y^2 + n_z^2 = 0 \tag{7b}$$

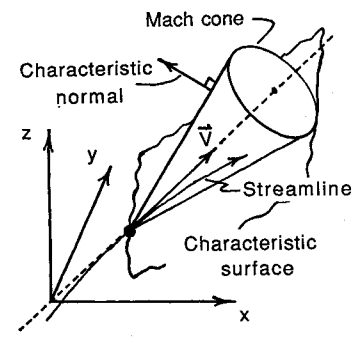

Fig. 1 Definition of characteristic surface and unit normal.

where either n_x, n_y, or n_z must be chosen, with the condition that $n_x \neq 0$. The three-dimensional compatibility equation given by Eq. (6), however, does not reduce to an ordinary differential equation as it does for the two-dimensional case. Reducing Eq. (6) to an ordinary differential equation is important for computational efficiency since it greatly simplifies the numerical implementation of the boundary condition. As an example, if the compatibility equation for the x-z plane were determined using Eq. (6) by setting $n_y = 0$, the result would be

$$\beta(-\beta u_x + u_z) + (-\beta w_x + w_z) + v_y = 0 \tag{8}$$

where the similarity parameter $\beta = \sqrt{M^2 - 1}$, which cannot be written as a total derivative because of the term involving v. For the two-dimensional steady full potential equation in the x-z plane, the compatibility equation is

$$\beta(-\beta u_x + u_z) + (-\beta w_x + w_z) = 0 \tag{9}$$

which can be written as the total derivative

$$\frac{\mathrm{d}}{\mathrm{d}s}\left(\beta u + w\right) = 0 \tag{10}$$

where $\mathrm{d}s$ is the element of length along a characteristic line (in this case a Mach line). Integrating Eq. (10) and switching to the small-disturbance potential function gives

$$\beta(1 + \phi_x) + \phi_z = \beta(1 + \phi_{x_\infty}) + \phi_{z_\infty} \tag{11}$$

or equivalently

$$\beta\phi_x + \phi_z = 0 \tag{12}$$

where Eq. (12) is called a Riemann invariant. Equation (12) is valid along the Mach lines where β depends on the local Mach number. To further simplify the boundary condition, β is set equal to a constant that is dependent only on the freestream Mach number (i.e., $\beta = \sqrt{M_\infty^2 - 1}$). It is this equation that was implemented as a boundary condition on the outer boundary of the grid in the CAP-TSD code. Comparison of the two- and three-dimensional compatibility equations for the x-z plane [Eqs. (8) and (9)] indicates that there is an extra term involving v_y in the three-dimensional equation. The error introduced by neglecting this term is small, as is shown in the results presented below. Similar boundary conditions are also derived for the x-y plane, and, thus, the new boundary conditions are

Above:

$$\beta\phi_x + \phi_z = 0 \tag{13a}$$

Below:

$$\beta\phi_x - \phi_z = 0 \tag{13b}$$

Far spanwise:

$$\beta\phi_x + \phi_y = 0 \tag{13c}$$

Note that in these equations, β approaches zero as the freestream Mach number goes to 1, resulting in the original boundary conditions of Eqs. (4). The downstream boundary condition was not changed since physically no information can propagate upstream for supersonic freestream flow. Previously, the boundary conditions [Eqs. (13a) and (13b)] were used by Chow and Goorjian[8] in a two-dimensional low-frequency TSD code known as LTRAN2. Later, Guruswamy and Goorjian[9] implemented these boundary conditions in the XTRAN3S Ames code. The far spanwise boundary condition of Eq. (13c), however, was not implemented in Ref. 9.

Results and Discussion

Calculations were performed for the NACA 0012 airfoil and the F-5 wing to assess the accuracy and efficiency of the supersonic far-field boundary conditions. In these calculations, two different sized sectional grids were used for the x-z plane. The first grid had boundaries located 20 chord lengths above and below the airfoil, 20 chord lengths upstream of the leading edge, and 20 chord lengths downstream of the trailing edge. The large grid extent was used to ensure that the far-field boundary conditions did not influence the surface pressures. This grid contained 140×92 points with 55 points located on the chord. The second grid had boundaries located 2.5 chord lengths above and below the airfoil, 2 chord lengths upstream of the leading edge, and 2 chord lengths downstream of the trailing edge. This grid is a subset of the larger grid and contains 109×62 points. The complete smaller grid is shown in Fig. 2. Both the large and small grids had extra points placed near the outer boundaries to more accurately approximate the outer boundary conditions. Using the small grid, parallel calculations were performed using both the original and supersonic boundary conditions to determine improvements in the solutions.

NACA 0012 Airfoil Results

Results were obtained for the NACA 0012 airfoil at several freestream Mach numbers and angles of attack. The first two cases studied correspond to a freestream Mach number of 1.2 with angles of attack of 0 and 7 deg. These two cases are AGARD[10] standard cases for assessment of inviscid flowfield methods. Comparisons are therefore made with the Euler calculations contained therein. Next, the effects of freestream Mach number were investigated for the range $1.0 \leq M_\infty \leq 2.0$. An unsteady case was also considered for the airfoil pitching harmonically about the quarter chord ($x_p = 0.25$) at a freestream Mach number of 1.2, a reduced frequency based on semichord of $k = 0.1$, and an oscillation amplitude of 1 deg about a mean angle of attack of 0 deg. The unsteady case was computed to determine how well the supersonic boundary conditions worked in a time-dependent calculation.

Case 1

The first case presented gives a comparison of steady pressure distributions computed using the large and small grids mentioned earlier. Figure 3 shows a comparison of the pressure distributions at $M_\infty = 1.2$ and $\alpha = 0$ deg. When using the supersonic boundary conditions, the solution calculated using the small grid is nearly identical to the solution using the large grid. Next, the small grid was used in calculating the effects of the two boundary conditions. Comparisons were also made with the published Euler results from Ref. 10. Figure 4 shows the steady pressure distributions obtained using the supersonic boundary conditions. These pressures are in very good agreement with the Euler results. Using the original boundary conditions, however, produces an erroneous increase in the surface pressure distribution.

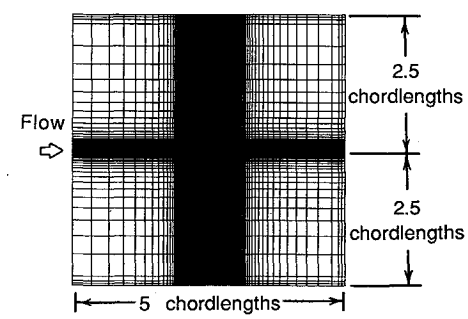

Fig. 2 Reduced sectional (x-z) finite-difference grid for CAP-TSD supersonic freestream calculations.

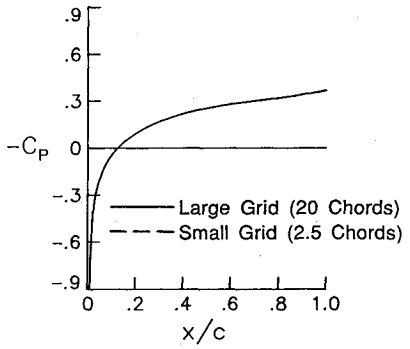

Fig. 3 Effects of grid extent on steady pressure distributions for the NACA 0012 airfoil at $M_\infty = 1.2$ and $\alpha = 0$ deg computed using the supersonic boundary conditions.

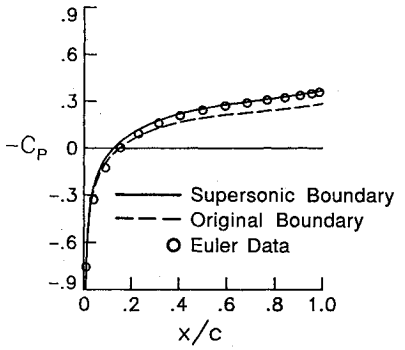

Fig. 4 Comparisons of steady pressure distributions for the NACA 0012 airfoil at $M_\infty = 1.2$ and $\alpha = 0$ deg computed using the small grid (2.5 chord lengths).

Case 2

Comparisons of pressure distributions are presented in Fig. 5, computed using the large and small grids. The results are for the more challenging case of $M_\infty = 1.2$ and $\alpha = 7$ deg. These results show that there is only a slight difference in the surface pressures when using the small grid and the supersonic boundary conditions. Calculations using the small grid and the two different boundary conditions are compared with the Euler results from Ref. 10 in Fig. 6. These comparisons indicate that using the supersonic boundary conditions results in surface pressures that are in good agreement with the Euler results, whereas the original boundary conditions cause the pressures to be overpredicted, especially along the lower surface.

Freestream Mach Number Effects

Comparisons are made between pressure distributions computed using the supersonic and original far-field boundary conditions at different Mach numbers. In all cases, the small grid was used. The purpose of these comparisons was to determine the effect of the supersonic boundary conditions as a function of freestream Mach number on the solutions. Figure 7 shows that at $M_\infty = 1.0$ there is no difference in the solutions. This is expected since $\beta = 0$ at $M_\infty = 1.0$ and the supersonic boundary conditions become identical to the original boundary conditions. As the Mach number is increased, the differences become greater until at some point the Mach lines become so highly swept that they no longer strike the upper or lower boundaries of the grid. Once this occurs, no disturbance from the airfoil reaches the outer far-field boundaries, and thus, at $M_\infty = 2.0$ the two sets of pressures are again identical to plotting accuracy. This implies that, as the Mach number is increased, the size of the grid could be continually reduced, within reason, without affecting the accuracy of the near-field solution.

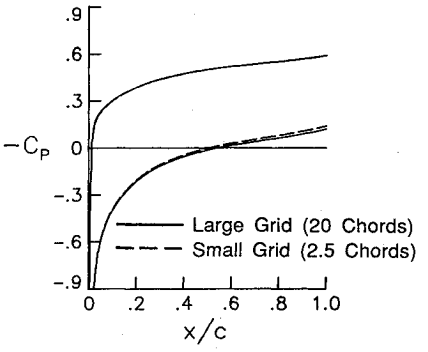

Fig. 5 Effects of grid extent on the steady pressure distributions of the NACA 0012 airfoil at $M_\infty = 1.2$ and $\alpha = 7$ deg computed using the supersonic boundary condition.

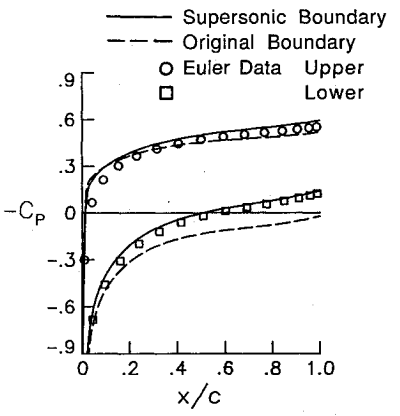

Fig. 6 Comparisons of steady pressure distributions for the NACA 0012 airfoil at $M_\infty = 1.2$ and $\alpha = 7$ deg computed using the small grid (2.5 chord lengths).

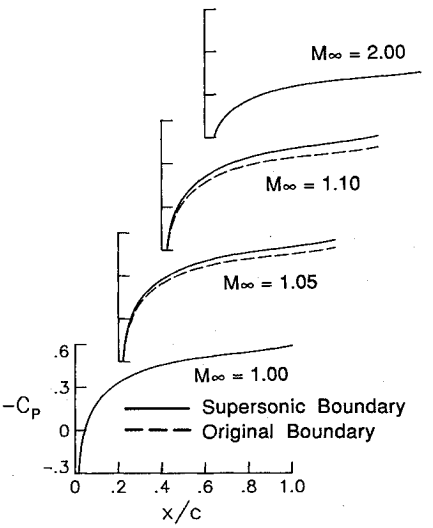

Fig. 7 Effects of the far-field boundary conditions on the steady pressure distributions for the NACA 0012 airfoil at $\alpha = 0$ deg and various Mach numbers computed using the small grid (2.5 chord lengths).

Unsteady Results

Comparisons are made between instantaneous pressure distributions using the supersonic and original boundary conditions for the NACA 0012 airfoil oscillating in pitch. Instantaneous surface pressures are shown at the maximum/minimum amplitude and when the amplitude is zero. Figure 8 shows that the pressure distributions computed using the large and small grids are virtually identical. Thus, the supersonic boundary conditions work well for unsteady as well as steady calculations, although Eqs. (13a–13c) are strictly valid only for steady

flows. Figure 9 shows that using the original boundary conditions with a small grid causes the pressures to be overpredicted.

F-5 Wing Results

Steady and unsteady calculations were also performed for the F-5 fighter wing to assess the new supersonic boundary conditions for three-dimensional applications. The F-5 planform is approximately 4% thick with a leading-edge sweep angle of 31.9 deg and a taper ratio of 0.28. The airfoil section is a modified NACA 65A004.8, which has a drooped nose and is symmetric aft of 40% chord. For the low supersonic Mach numbers, a suction peak in the pressure coefficient exists on the lower surface near the leading edge. Experimental data[11] are available and are used for comparison. The grid used in the x-z plane is identical to the one used for the NACA 0012 case. The grid points are distributed in the spanwise direction according to a cosine distribution that clusters points near the tip. Twenty points were used on the wing span and 20 points were included in the outboard region. The number of grid points used is $109\times40\times62$ for the small grid and $140\times40\times92$ for the large grid. The computational cost for the unsteady results using the large grid was approximately 3600 CPU s on the CRAY2 computer at the Numerical Aerodynamic Simulator located at NASA Ames Research Center, as compared to approximately 1900 CPU s for the small grid. Calculations on both grids were performed with a step size of 0.0715, giving 360 steps/cycle of motion with a total of 2160 steps. Six cycles of motion were computed to ensure a periodic solution.

In addition to the preceding calculations, the effects of grid refinement were studied at one Mach number for both steady and unsteady flows. The same small grid discussed previously was used except that the number of points along the chord was approximately doubled to give 109 points on the chord. This resulted in a grid size of $163\times40\times62$.

Case 1

Steady pressure distributions were calculated using the supersonic and original boundary conditions with the small grid. Comparisons were then made between these two sets of results and experimental data. The results shown in Fig. 10 demonstrate the need for the supersonic boundary conditions. For all span stations, the original boundary conditions cause the pressure distributions to be overpredicted. Figure 10 also shows that the suction peak is predicted well due to using the $109\times40\times62$ grid. Results published in many previous TSD papers have not predicted the suction peak for the F-5 wing very well. The reason for the good agreement here is the fine grid in the leading-edge region of the wing (see Fig. 2). Comparisons were also made between the pressure distributions calculated using the supersonic boundary conditions with the large and small grids. The results were identical to plotting accuracy and, hence, are not shown here. Use of the supersonic boundary conditions for this case allows a more accurate solution to be obtained on smaller computational grids.

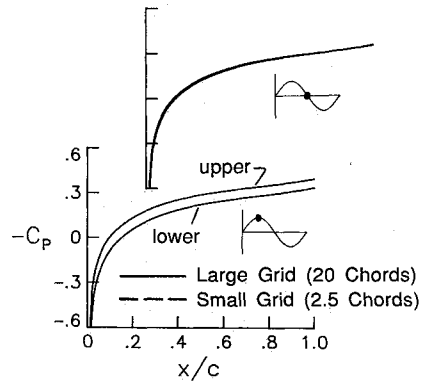

Fig. 8 Effects of grid extent on the instantaneous pressure distributions for the NACA 0012 airfoil at $M_\infty = 1.2$, $k = 0.1$, $x_p = 0.25$, $\alpha_m = 0$ deg, and $\alpha_o = 1$ deg.

Case 2

Unsteady pressure distributions were computed using the original and supersonic boundary conditions on the small grid. The experimental model was oscillated about the root midchord with an amplitude of 0.552 deg about a mean angle of attack of 0 deg. The freestream Mach number was 1.05 and the reduced frequency based on root semichord of 0.1. The first vibration mode of the wing was used in the unsteady calculations to account for a small amount of flexibility in the experimental model. This was done because the node line is not normal to the root chord but bends back significantly at this Mach number. Comparisons between the pressure distributions using the original and supersonic boundary conditions are shown in Fig. 11. The supersonic boundary conditions have greatly improved the accuracy of the solution in comparison with experiment, whereas the original boundary conditions give much larger unsteady pressures than is predicted by the experiment.

Comparisons of the computed upper surface unsteady pressure distributions and the experimental data show good agreement except near the tip. When the lower surface unsteady pressure distributions are compared with experiment, good agreement is found all along the span. Also, the computed results predict accurately the peaks in the unsteady pressures.

As before, the large grid solution can be used to judge the accuracy of the small grid solution since it should be independent of the far-field boundary conditions used. Although the results are not shown, the solutions obtained using the large grid and the small grid (with the supersonic boundary conditions) are virtually identical to plotting accuracy.

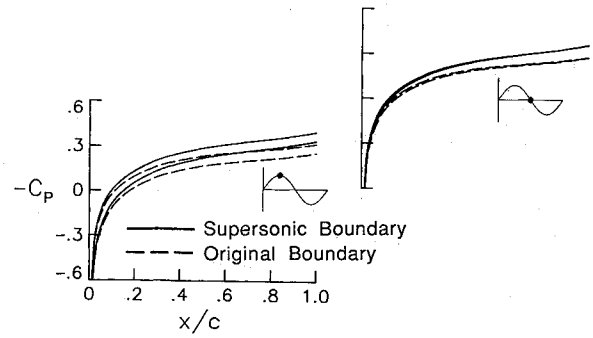

Fig. 9 Effects of the far-field boundary conditions on instantaneous pressure distributions for the NACA 0012 airfoil at $M_\infty = 1.2$, $k = 0.1$, $x_p = 0.25$, $\alpha_m = 0$ deg, and $\alpha_o = 1$ deg.

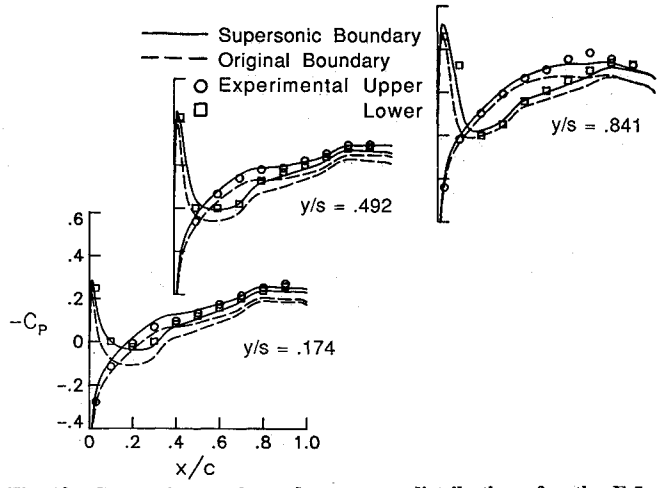

Fig. 10 Comparisons of steady pressure distributions for the F-5 wing at $M_\infty = 1.05$ and $\alpha = 0$ deg computed using the small grid (2.5 chord lengths).

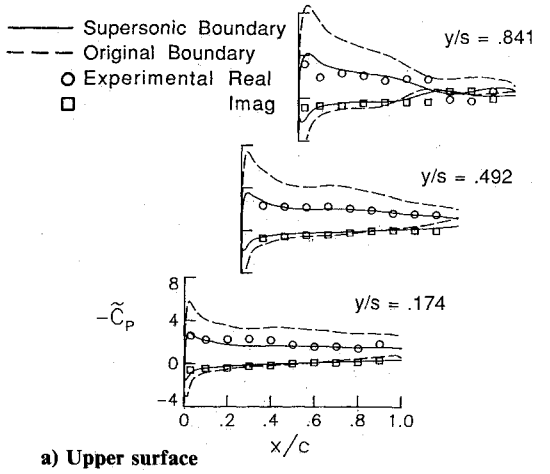

a) Upper surface

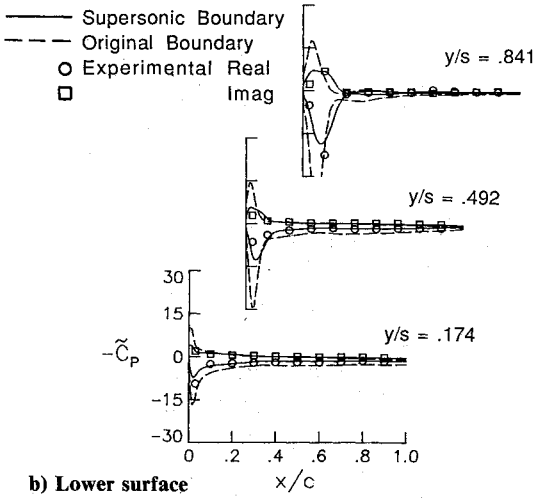

b) Lower surface

Fig. 11 Comparisons of unsteady pressure distributions for the F-5 wing at $M_\infty = 1.05$, $k = 0.1$, $x_p = 0.50$, $\alpha_m = 0$ deg, and $\alpha_o = 0.552$ deg computed using the original and supersonic boundary conditions.

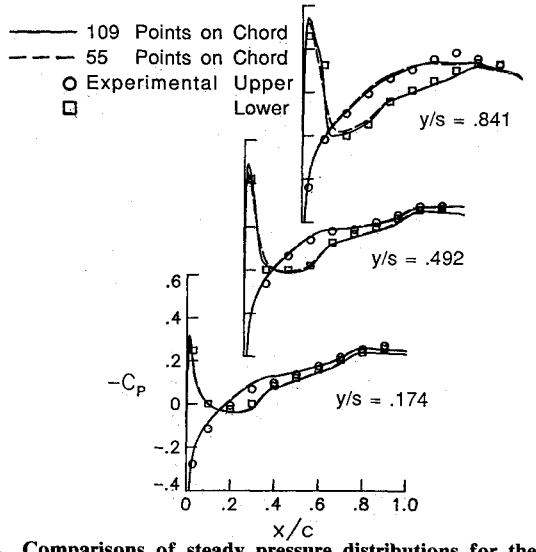

Fig. 12 Comparisons of steady pressure distributions for the F-5 wing at $M_\infty = 1.05$ and $\alpha = 0$ deg showing grid refinement effects.

Case 3

Both steady and unsteady results are shown, obtained using a different number of grid points, although the grid extents are the same as the small grid discussed earlier. The only difference in the two grids is the number of points placed along the chord. The medium-sized grid has 55 points along the chord and the fine grid has 109 points along the chord. The

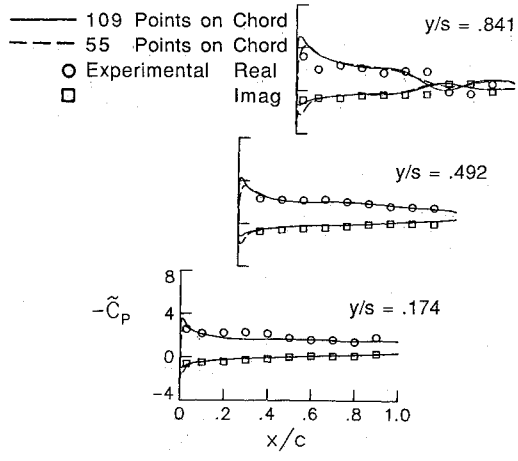

a) Upper surface

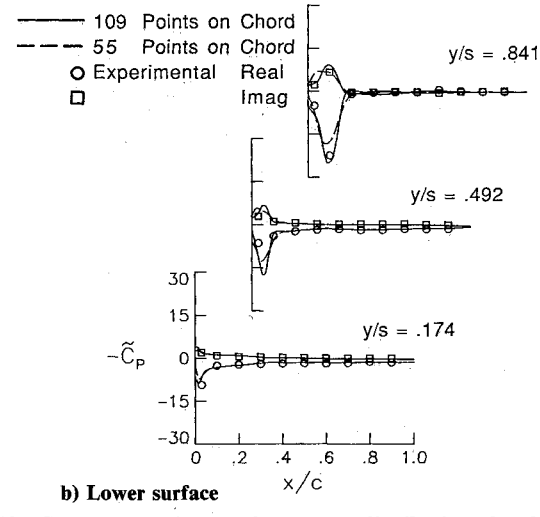

b) Lower surface

Fig. 13 Comparison of unsteady pressure distributions for the F-5 wing at $M_\infty = 1.05$, $k = 0.1$, $x_p = 0.50$, $\alpha_m = 0$ deg, and $\alpha_o = 0.552$ deg showing grid refinement effects.

supersonic boundary conditions were used in all of the calculations.

Comparisons of steady pressure distributions are shown in Fig. 12 for the F-5 wing at $M_\infty = 1.05$ and $\alpha = 0$ deg. The main difference in the medium and fine grid solutions is the well-defined suction peak. The better resolution of the suction peak for the steady case has an influence on the unsteady pressures as shown in Fig. 13. For example, the unsteady pressures on the lower surface (Fig. 13b) show that the fine grid produces much larger unsteady pressures near the leading edge, which are in better agreement with the experimental pressures.

Concluding Remarks

Characteristic far-field boundary conditions for supersonic freestream flow have been developed and implemented within the CAP-TSD transonic small-disturbance code. To assess the improvements in the solutions, calculations were performed for a NACA 0012 airfoil and an F-5 fighter wing. The calculations were performed using two different grids in the x-z plane. A large grid was used for comparisons since the surface pressures should be independent of the far-field boundary conditions. A small grid was used to demonstrate the effectiveness of the supersonic boundary conditions.

Steady and unsteady results were calculated for the NACA 0012 airfoil and compared with Euler results where available.

The use of the supersonic boundary conditions allowed a much smaller grid to be used and improved the accuracy of the solutions for supersonic freestream applications. The results obtained using the supersonic boundary conditions were shown to differ from the original boundary conditions only over a small range of freestream Mach numbers, for the cases considered. This range of difference is located at low supersonic Mach numbers near $M_\infty = 1.0$. Thus, the supersonic boundary conditions are particularly important for low supersonic cases.

The steady results for the F-5 wing indicate that the supersonic boundary conditions allow a much smaller grid to be used without losing accuracy and, in this case, decrease the computational cost by a factor of approximately two. Comparisons of the pressure distributions with experimental data showed that the supersonic boundary conditions resulted in much better agreement with experiment than pressures obtained using the original boundary conditions.

Unsteady flow calculations for the F-5 wing indicate that the supersonic boundary conditions can be used for time accurate calculations of three-dimensional flows. Finally, the grid refinement results indicate that better agreement with experiment can be obtained by using a finer grid, which is an expected result.

References

[1]Edwards, J. W., and Thomas, J. L.,"Computational Methods for Unsteady Transonic Flows," AIAA Paper 87-0107, Jan. 1987.

[2]Batina, J. T., Seidel, D. A., Bland, S. R., and Bennett, R. M., "Unsteady Transonic Flow Calculations for Realistic Aircraft Configurations," *Journal of Aircraft*, Vol. 26, No. 1, 1989, pp. 21-28.

[3]Batina, J. T., "Unsteady Transonic Small-Disturbance Theory Including Entropy and Vorticity Effects," *Journal of Aircraft*, Vol. 26, No. 6, 1989, pp. 531-538.

[4]Bennett, R. M., Bland, S. R., Batina, J. T., Gibbons, M. D., and Mabey, D. G., "Calculations of Steady and Unsteady Pressures on Wings at Supersonic Speeds with a Transonic Small Disturbance Code," AIAA Paper 87-0851, April 1987.

[5]Kwak, D., "Non-Reflecting Far-Field Boundary Conditions for Unsteady Transonic Flow Computations," AIAA Paper 80-1393, 1980.

[6]Batina, J. T., "Unsteady Transonic Algorithm Improvements for Realistic Aircraft Applications," *Journal of Aircraft*, Vol. 26, No. 2, 1989, pp. 131-139.

[7]Zucrow, M. J., and Hoffman, J. D., *Gas Dynamics Multidimensional Flow*, Vol. 2, Wiley, New York, 1977.

[8]Chow, L. J., and Goorjian, P. M.,"Implicit Unsteady Transonic Airfoil Calculations at Supersonic Freestreams," AIAA Paper 82-0934, June 1982.

[9]Guruswamy, G. P., and Goorjian, P. M., "Unsteady Transonic Aerodynamics and Aeroelastic Calculations at Low-Supersonic Freestreams," *Journal of Aircraft*, Vol. 25, No. 10, 1988, pp. 955-961.

[10]Yoshihara, H., "Test Cases for Inviscid Flow Field Methods," AGARD-AR-211, May 1985.

[11]Tijdeman, H., Van Nunen, J. W. G., Kraan, A. N., Persoon, A. J., Poestkoke, R., Roos, R., Schippers, P., and Siebert, C. M., "Transonic Wind Tunnel Tests on an Oscillating Wing with External Stores," AFFDL-TR-78-194, Dec. 1978.